The dissociation/recombination reaction CH4 (+M) CH3 + H (+M): A case study for unimolecular rate theory

J. Troe and V. G. Ushakov

Citation: J. Chem. Phys. **136**, 214309 (2012); doi: 10.1063/1.4717706
View online: http://dx.doi.org/10.1063/1.4717706
View Table of Contents: http://jcp.aip.org/resource/1/JCPSA6/v136/i21
Published by the American Institute of Physics.

The dissociation/recombination reaction CH_4 (+M) ⇔ CH_3 + H (+M): A case study for unimolecular rate theory

J. Troe[1,2,a] and V. G. Ushakov[2,3]
[1]*Institute for Physical Chemistry, University of Göttingen, Tammannstrasse 6, D-37077 Göttingen, Germany*
[2]*Max-Planck-Institute for Biophysical Chemistry, Am Fassberg 11, D-37077 Göttingen, Germany*
[3]*Institute of Problems of Chemical Physics, Russian Academy of Sciences, 142432 Chernogolovka, Russia*

(Received 28 March 2012; accepted 29 April 2012; published online 6 June 2012)

The dissociation/recombination reaction CH_4 (+M) ⇔ CH_3 + H (+M) is modeled by statistical unimolecular rate theory completely based on dynamical information using *ab initio* potentials. The results are compared with experimental data. Minor discrepancies are removed by fine-tuning theoretical energy transfer data. The treatment accounts for transitional mode dynamics, adequate centrifugal barriers, anharmonicity of vibrational densities of states, weak collision and other effects, thus being "complete" from a theoretical point of view. Equilibrium constants between 300 and 5000 K are expressed as $K_c = k_{rec}/k_{dis} = \exp(52\ 044\ \mathrm{K}/T)\ [10^{-24.65}\ (T/300\ \mathrm{K})^{-1.76} + 10^{-26.38}\ (T/300\ \mathrm{K})^{0.67}]\ \mathrm{cm}^3\ \mathrm{molecule}^{-1}$, high pressure recombination rate constants between 130 and 3000 K as $k_{rec,\infty} = 3.34 \times 10^{-10}\ (T/300\ \mathrm{K})^{0.186} \exp(-T/25\ 200\ \mathrm{K})\ \mathrm{cm}^3\ \mathrm{molecule}^{-1}\ \mathrm{s}^{-1}$. Low pressure recombination rate constants for M = Ar are represented by $k_{rec,0} = [\mathrm{Ar}]\ 10^{-26.19} \exp[-(T/21.22\ \mathrm{K})^{0.5}]\ \mathrm{cm}^6\ \mathrm{molecule}^{-2}\ \mathrm{s}^{-1}$, for M = N_2 by $k_{rec,0} = [\mathrm{N_2}]\ 10^{-26.04} \exp[-(\mathrm{T}/21.91\ \mathrm{K})^{0.5}]\ \mathrm{cm}^6\ \mathrm{molecule}^{-2}\ \mathrm{s}^{-1}$ between 100 and 5000 K. Weak collision falloff curves are approximated by asymmetric broadening factors [J. Troe and V. G. Ushakov, J. Chem. Phys. **135**, 054304 (2011)] with center broadening factors of $F_c \approx 0.262 + [(T - 2950\ \mathrm{K})/6100\ \mathrm{K}]^2$ for M = Ar. Expressions for other bath gases can also be obtained. © *2012 American Institute of Physics*. [http://dx.doi.org/10.1063/1.4717706]

I. INTRODUCTION

The dissociation/recombination reaction

$$\mathrm{CH_4(+M)} \Leftrightarrow \mathrm{CH_3 + H(+M)} \qquad (1.1)$$

continues to be chosen as a test system for reaction rate theories. The practical importance of the system needs not to be emphasized. As a consequence, there is an experimental database of a certain size, see, e.g., the summaries and evaluations in Refs. 1 and 2. However, in spite of the relatively large number of experimental studies, the database is incomplete and the last experimental work published to our knowledge dates back to 2001.[3] Particularly scarce are data close to the limiting low and high pressure ranges which cover a sufficiently broad part of the falloff curve such that reliable extrapolations to the limits can be made. In this situation, improved *ab initio* quantum chemical calculations of intra- and intermolecular potential energy surfaces are of particular help to define the properties of the rate constants.[4–7] In particular, the moderate increase of the high pressure recombination rate constant $k_{rec,\infty}$ from values near 3×10^{-10} at 300 K to 3.5×10^{-10} $\mathrm{cm}^3\ \mathrm{molecule}^{-1}\ \mathrm{s}^{-1}$ at 1500 K could be reproduced and the influence on $k_{rec,\infty}$ of various calculational approaches to the potential was demonstrated.[4,5] Calculations on the CASPT2/aug-cc-pVDZ level of theory apparently were sufficiently reliable to calculate $k_{rec,\infty}$ with "kinetic accuracy."

Taking advantage of the *ab initio* potential energy calculations, one may go one step further and employ the results for calculations of complete falloff curves of the reaction. This is the aim of the present work, extending the studies from Refs. 4–7. Different from earlier work,[4,5] we now calculate classical trajectories for capture of H by CH_3. We then combine the results for the dynamics on the reduced-dimensionality *ab initio* potential of the transitional modes with the contributions from the conserved modes, i.e., we use the statistical adiabatic channel model/classical trajectories approach (SACM/CT) outlined in Refs. 8–11. Finally, we incorporate the results into general expressions for broadening factors of unimolecular reactions[12,13] and compare the results with new analytical approximations for the rate constants as proposed in Ref. 14. The described treatment, for strong collisions, may be considered as approaching a certain degree of completeness. It treats the transitional mode dynamics on an intramolecular *ab initio* potential, accounts for the radial and anisotropic properties of the potential, accounts for rotational effects and also includes anharmonicity models for the density of states. By doing this, it goes beyond earlier more empirical approaches such as the simplified SACM modeling of the falloff curves of reaction (1.1) recommended in Ref. 2 on the basis of the analysis from Ref. 15, or the Rice-Ramsperger-Kassel-Marcus (RRKM)/master equation modeling from Ref. 16, which both arrived at falloff curves with different broadening factors than suggested in the present work, see below.

The modeling of the falloff curves and the limiting low pressure rate constants for recombination and dissociation, $k_{rec,0}$ and $k_{dis,0}$, respectively, generally left the average (total) energy $\langle \Delta E \rangle$ transferred per collision as a fit parameter. Analyzing experimental values of $k_{dis,0}$ between 1000 and

[a]Author to whom correspondence should be addressed. Electronic mail: shoff@gwdg.de.

5000 K for M = Ar, e.g., $-\langle\Delta E\rangle/hc \approx 50\ (\pm 20)\ cm^{-1}$ was fitted in Ref. 17 independent of the temperature. Taking into account that $\langle\Delta E\rangle$ is approximately related to the average energy $\langle\Delta E_d\rangle$ transferred per down collision through[18] $\langle\Delta E\rangle \approx -\langle\Delta E_d\rangle^2/(\langle\Delta E_d\rangle + F_E kT)$ (with F_E being related to the energy dependence of the density of states, see below), recent classical trajectory results for $\langle\Delta E_d\rangle$ in collisions between CH_4 and M (Refs. 6, 7, 19, and 20) within a factor of about two agreed with the results from Ref. 17 (the most detailed work from Ref. 7 led to $\langle\Delta E_d\rangle/hc = 115\ cm^{-1}\ (T/300\ K)^{0.75}$ which with[21] $F_E = 1.31$ gives $-\langle\Delta E\rangle/hc = 99\ cm^{-1}$ for $T = 2000$ K). As there were several relatively uncertain contributions in the analysis of experimental values of $k_{dis,0}$ from Ref. 17, see below, this confirms the expectation that $\langle\Delta E\rangle$-values derived from the experiments are accurate within about a factor of two. The present work allowed us to improve the analysis of low pressure rate constants and to put the comparison of theoretical and experimental values of $\langle\Delta E\rangle$ or $\langle\Delta E_d\rangle$ on a safer basis. In addition to this, we also try to make predictions for the bath gases M = O_2 and H_2O not treated in Ref. 7. Here, we rely on experience obtained in previous work[22] on the reaction H + O_2 (+M) → HO_2 (+M) with M = H_2O.

II. TRAJECTORY CALCULATIONS FOR CAPTURE OF H BY CH_3

Our calculation of the recombination rate constants k_{rec} for the reaction H + CH_3 (+M) → CH_4 (+M) closely follows the SACM/CT methodology elaborated, e.g., in Ref. 10. We first consider the dynamics of the transitional modes which, at large H–CH_3 distance, correspond to free rotations of CH_3 relative to H and translation of H towards CH_3. The starting conditions for trajectories are randomly chosen from uniform phase space distributions over the quantum numbers *j, k,* and *L* (for fixed *J* and *E*), obeying all angular momentum constraints (CH_3 is approximately represented by a planar oblate symmetrical top with the rotational constants B ≈ C and A ≈ B/2 and the quantum numbers *j* and *k*; as the effective bottleneck of the reaction is at large H–CH_3 distances, the use of planar CH_3 appears fully justified; *L* corresponds to the orbital angular momentum, *J* to the total angular momentum, and *E* to the total energy of the system; zero energy is put at the rovibrational ground state of CH_3). Trajectories are followed until capture or failure of capture is obtained. Capture is assumed to be achieved when the H–CH_3 distance is smaller than the minimum of the sum of the radial and centrifugal potential, being of the order of 3 a.u. More than 10^4 trajectories were run for each pair (*E, J*) such that the resulting capture probability had less than about 2% statistical error. By determining capture probabilities *w*(*E, J*), for the number of entrance channels of the transitional modes $W_0(E, J)$, the number of open channels of the transitional modes $W_{tr}(E, J)$ for recombination is expressed as

$$W_{tr}(E, J) = w(E, J) W_0(E, J). \tag{2.1}$$

By convoluting $W_{tr}(E, J)$ with the number of states of the conserved modes of CH_3, the total number of open channels $W(E, J)$ for recombination finally is given by

$$W(E, J) = \sum_{i=0}^{\infty} W_{tr}(E - E_i, J), \tag{2.2}$$

where *E* now corresponds to the total energy of the formed CH_4 and the summation goes over all vibrational states E_i of CH_3 taken as conserved modes. Besides capture probabilities *w*(*E, J*) for the complete anisotropic potential, we also calculate capture probabilities $w^{PST}(E, J)$ for a potential omitting anisotropy such as assumed in phase space theory (PST). The comparison gives *E*- and *J*-specific rigidity factors

$$f_{rig}(E, J) = w(E, J)/w^{PST}(E, J). \tag{2.3}$$

(The molecular parameters used in our calculations are summarized in the Appendix.) We used two potential energy surfaces for our calculations. The first was the *ab initio* CASPT2 potential in its ADZ and ATZ versions kindly provided by L. B. Harding,[23] as also employed in Refs. 4 and 5. The potential is characterized by a Morse-type radial potential along the H–CH_3 bond and it has a relatively weak anisotropy. We also tested a second potential, where the radial part on the basis of the full-CI *ab initio* calculations of Ref. 24 was fitted to a Morse potential and the anisotropy was taken of simple model character,

$$V(r, \theta) = D\{\exp[-2\beta(r - r_e)] - 2\exp[-\beta(r - r_e)]\} + C\exp[-\beta(r - r_e)]\sin^2(\theta - \pi/2) \tag{2.4}$$

with a fitted Morse parameter β, the dissociation energy *D*, the H–CH_3 distance *r*, and the angle θ between the H–CH_3 line and the CH_3 plane (an influence of the additional azimuthal angle φ was also tested but found unimportant). For simplicity, we term this potential the "full-CI Morse potential." Figure 1 compares the radial parts of the "full-CI Morse potential" (with the fitted parameters *D*/hc = 39 450 cm^{-1}, $\beta = 1.086$ a.u.$^{-1}$ and $r_e = 2.135$ a.u.) and of the CASPT2(ATZ) potential. The agreement between the

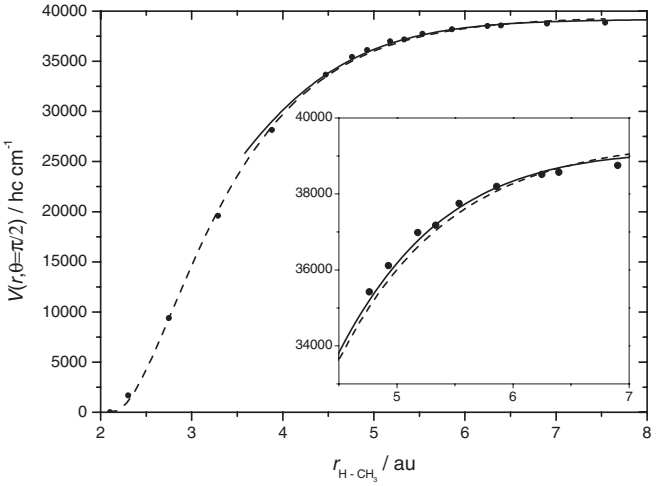

FIG. 1. Radial potential for H–CH_3 (points: full-CI *ab initio* calculations from Ref. 24; dashed line: Morse fit to the points with *D*/hc = 39 450 cm^{-1}, $\beta = 1.086$ a.u.$^{-1}$, and $r_e = 2.135$ a.u.; solid line: CASPT2 (ATZ) potential from Refs. 4, 5, and 23).

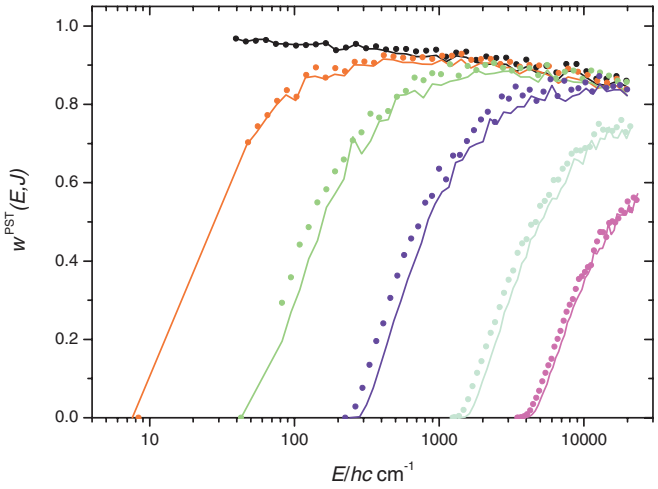

FIG. 2. Capture probabilities $w^{PST}(E, J)$ for isotropic potentials (PST = phase space theory; points: "full-CI Morse potential" of Eq. (2.4); lines: CASPT2 (ATZ) potential; results from right to left for $J = 60$, 40, 20, 10, 5, and 0).

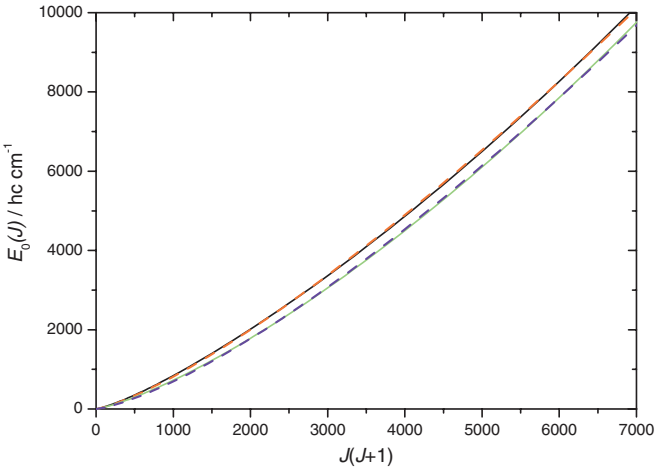

FIG. 3. Centrifugal barriers $E_0(J)$ for the CASPT2 (ATZ) potential (upper lines) and the "full-CI Morse potential" of Eq. (2.4) (lower lines) (solid lines = numerical results, dashed lines: representation by Eq. (2.5)).

variants of the radial potential appears quite satisfactory, although the CASPT2(ATZ) potential has the tendency to be slightly high at $r < 2.5$ a.u., see later on. The anisotropy parameter C of Eq. (2.4) was fitted *a posteriori* in such a way that the high pressure recombination rate constant $k_{rec,\infty}$ from calculations with the CASPT2 potential was reproduced (the ratio C/D was found to be close to 2.5, see below; as before,[10] we have used the ratio C/D to characterize the overall anisotropy of the potential with respect to capture dynamics).

Illustrating the results of our trajectory calculations, we first show PST capture probabilities $w^{PST}(E, J)$, obtained by omitting the anisotropy of the potential. Figure 2 compares results for the CASPT2(ATZ) potential with results for the "full-CI Morse potential" of Eq. (2.4). With increasing J, the onset of the curves at the centrifugal barriers $E_0(J)$ is slightly shifted towards larger energies for the CASPT2 potential. Apart from these minor differences due to slightly different centrifugal barriers, the results almost agree.

The centrifugal barriers can very well be represented in the form[25]

$$E_0(J) \approx Cv[J(J+1)]^v \tag{2.5}$$

with the parameters $C_v/\mathrm{hc} = 0.142$ cm^{-1} and $v = 1.258$ at $J \leq 44$ ($C_v/\mathrm{hc} = 0.109$ cm^{-1} and $v = 1.292$ at $J > 44$) for the CASPT2(ATZ) potential, while $C_v/\mathrm{hc} = 0.0972$ cm^{-1} and $v = 1.291$ at $J \leq 46$ ($C_v/\mathrm{hc} = 0.0604$ cm^{-1} and $v = 1.354$ at $J > 46$) for the "full-CI Morse potential". Figure 3 illustrates the quality of Eq. (2.5). One should note that, because of the small reduced mass of the H + CH_3-system, $E_0(L)$ and $E_0(J)$ are not identical (replacing J by L in Eq. (2.5), one has $C_v/\mathrm{hc} = 0.112$ cm^{-1} and $v = 1.323$ at $L \leq 49$, and $C_v/\mathrm{hc} = 0.0241$ and $v = 1.519$ at $L > 49$ for the CASPT2(ATZ) potential, while $C_v/\mathrm{hc} = 0.0599$ cm^{-1} and $v = 1.389$ at $J \leq 52$, and $C_v/\mathrm{hc} = 0.00505$ cm^{-1} and $v = 1.701$ at $L > 52$ for the "full-CI Morse potential"). Having the parameters C_v and v facilitates the analysis of rotational contributions to specific rate constants $k(E, J)$, high pressure, and low pressure rate constants as shown in Secs. III–VII.

Figure 4 presents capture probabilities $w(E, J)$ for the complete anisotropic potential. Results for the CASPT2(ATZ) and the "full-CI Morse potential" are compared. The general agreement between the two approaches is quite good although some differences are noted for small J. Apparently in this detail, the model anisotropy of Eq. (2.4) oversimplifies the real anisotropy (better represented by the CASPT2 potential), although much of this effect later on is averaged out. Figure 5 continues the illustration of our results by showing the rigidity factors of Eq. (2.3) for the CASPT2(ATZ) potential, i.e., by combining Figs. 2 and 4. The values for all J with increasing E approach a common curve, which slowly decays from unity at small energies to smaller values at larger energies. Only close to the centrifugal barriers $E_0(J)$ more pronounced anisotropy effects (i.e., smaller rigidity factors) are noticed. It should be mentioned that the common high energy part of all curves resembles an expression of the type

$$f_{rig}(E) \approx \exp(-E/c), \tag{2.6}$$

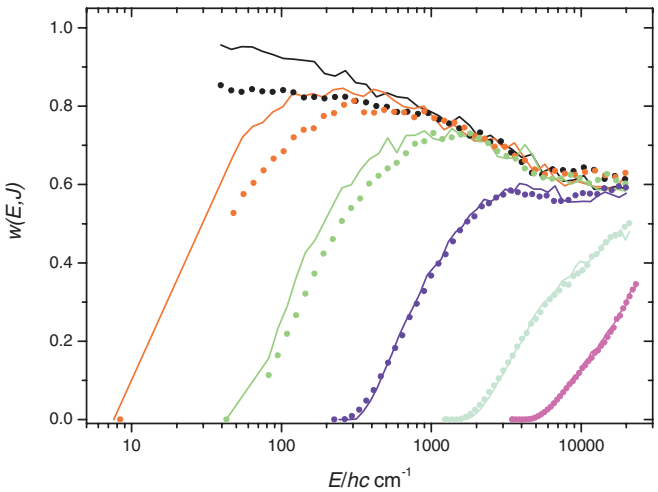

FIG. 4. Capture probabilities $w(E, J)$ for the full anisotropic potentials (points and lines as in Fig. 2).

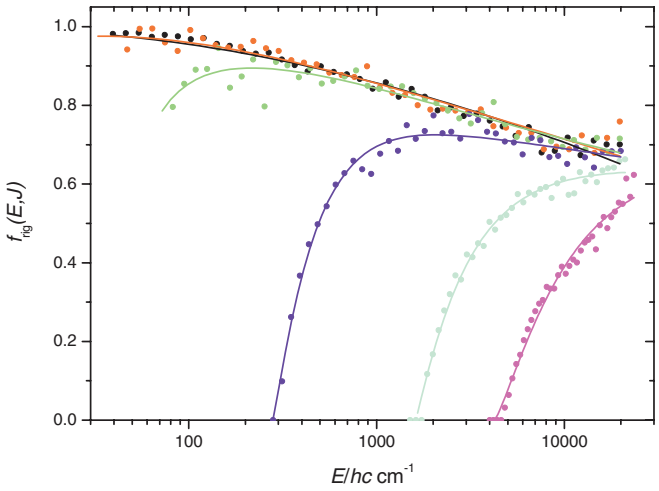

FIG. 5. Specific rigidity factors $f_{rig}(E, J)$ from Eq. (2.3), obtained by combining Figs. 2 and 4 (points and lines as in Figs. 2 and 4).

which successfully was used in the SSACM (simplified SACM) representation of specific rate constants $k(E, J)$ of cation dissociations in Ref. 26. For simple bond fission reactions, as a general rule, PST is approached near threshold and specific rate constants increasingly fall below PST values with increasing energy until results from rigid activated complex theory are finally approached.[27]

III. HIGH PRESSURE RECOMBINATION RATE CONSTANTS $k_{rec,\infty}$ FOR H + CH_3 → CH_4

A transparent analysis of the limiting high pressure rate constants for recombination $k_{rec,\infty}$ can be performed when first the PST expression is considered, given by

$$k_{rec,\infty}^{PST} = \left(\frac{kT}{h}\right)\left(\frac{h^2}{2\pi\mu kT}\right)^{3/2}\frac{Q_{el}(CH_4)\,Q_{cent}}{Q_{el}(H)\,Q_{el}(CH_3)} \quad (3.1)$$

with the centrifugal partition function

$$Q_{cent} = \sum_{L=0}^{\infty}(2L+1)\exp[-E_0(L)/kT]. \quad (3.2)$$

The latter can either be evaluated with numerical values for $E_0(L)$ or, if Eq. (2.5) holds with J replaced by L, in analytical form[25]

$$Q_{cent} = \Gamma(1+1/\nu)\,[kT/C_\nu]^{1/\nu}. \quad (3.3)$$

Our numerical calculations of $k_{rec,\infty}^{PST}$ through capture probabilities on the potential surfaces omitting anisotropy and through the analytical form of Eqs. (3.1)–(3.3) fully agreed. The comparison thus provides a useful test for "dynamical" vs "statistical" rate constants.

Accounting for the anisotropy of the potential surface reduces $k_{rec,\infty}$ relative to the PST results $k_{rec,\infty}^{PST}$. One may describe this by the thermal rigidity factor $f_{rig}(T)$,

$$k_{rec,\infty} = f_{rig}(T)k_{rec,\infty}^{PST}, \quad (3.4)$$

which is related to the E- and J-specific rigidity factor $f_{rig}(E, J)$ shown in Fig. 5, see below. The complete rate constant $k_{rec,\infty}$ analogous to Eq. (3.1) is given by

$$k_{rec,\infty} = \left(\frac{kT}{h}\right)\left(\frac{h^2}{2\pi\mu kT}\right)^{3/2}\frac{Q_{el}(CH_4)}{Q_{el}(H)\,Q_{el}(CH_3)}Q^*, \quad (3.5)$$

where Q^* replaces Q_{cent}. Q^* is given by

$$Q^* = \sum_{J=0}^{\infty}(2J+1)\int_{E_0(J)}^{\infty}W_{tr}(E,J) \times \exp(-E/kT)dE/(kT\,Q_{rot}^*(CH_3)) \quad (3.6)$$

and where the number of open channels for the transitional modes $W_{tr}(J) = w(E, J)W_0(E, J)$ is from Sec. II (see Fig. 4) and $Q_{rot}^*(CH_3)$ is the rotational partition function of CH_3 in oblate symmetrical top approximation (omitting or including symmetry numbers $\sigma = 6$ both in $Q_{rot}^*(CH_3)$ and in $W_{tr}(E, J)$). Figure 6 compares the finally obtained values of $k_{rec,\infty}$ with $k_{rec,\infty}^{PST}$. The "full-CI Morse" and CASPT2(ATZ) results for $k_{rec,\infty}^{PST}$, because of slightly different centrifugal barriers $E_0(L)$, are slightly different. We have, in part, compensated this by the choice of our fitted "global anisotropy parameter" $C/D = 2.5$ in Eq. (2.4) for which k_{rec}^{∞} is also shown in the figure. The comparison of $k_{rec,\infty}$ and $k_{rec,\infty}^{PST}$ indicates thermal rigidity factors of 0.75 at 300 K decreasing to 0.56 at 3000 K. The reaction thus is characterized by only mild anisotropy of the potential. This corresponds to the conclusions also drawn from the specific rigidity factors shown in Fig. 5.

Figure 7 compares a variety of calculations of $k_{rec,\infty}$, i.e., with CASPT2(ADZ), CASPT2(ATZ), and "full-CI Morse potentials" (with the parameter $C/D = 2.5$ in Eq. (2.4) and capture radii $r_{capt} = 2.97$ a.u. or $r_{capt} = 3.6$ a.u.). All results agree well up to about 1000 K whereas minor differences (less than 10%) become apparent at higher temperatures. These, however, appear irrelevant for practical applications, because medium to low pressure conditions are most typical in practice at high temperatures, see below. The figure also contains transition state theory (TST) result on the CASPT2(ADZ) potential from Refs. 4 and 5 which accounted for dynamical recrossing by a factor of 0.9 independent of the temperature. This factor was obtained by analyzing trajectories starting at the critical surface. By putting a limit between recrossing and non-recrossing trajectories at a H–CH_3 distance of 2.8 a.u., a recrossing factor of 0.9 was obtained. According to Fig. 1, the H–CH_3 distance of 2.8 a.u. is in a range where the CASPT2 potential of Refs. 4 and 5 is slightly high. This does not influence the resulting values of $k_{rec,\infty}$ up to 500 K where the present trajectory and the recrossing-corrected TST results agree very well. However, for higher temperatures the amount of recrossing from the CASPT2 potential apparently is overestimated and the recrossing-corrected TST values fall below our results.

When fitted to a simple power law, the CASPT2(ATZ) results of Fig. 6 between 100 and 2000 K are well represented by

$$k_{rec,\infty} \approx 3.34\times10^{-10}(T/300\text{K})^{0.15}\text{cm}^3\,\text{molecule}^{-1}\,\text{s}^{-1} \quad (3.7)$$

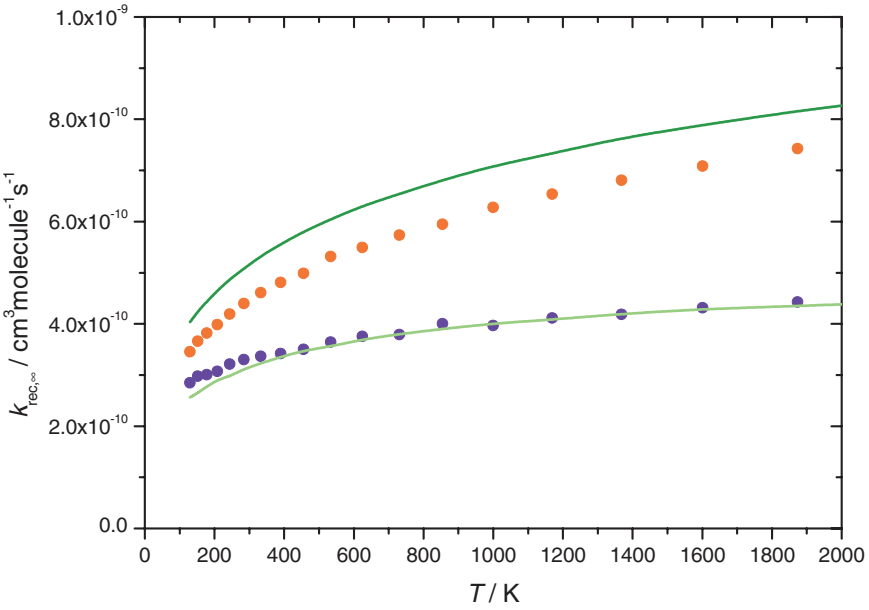

FIG. 6. Limiting high pressure recombination rate constants $k_{rec,\infty}$ (from top to bottom: upper solid line: PST results for isotropic "full-CI Morse potential" of Eq. (2.4); upper points: PST results for isotropic CASPT2 (ATZ) potential; lower points: anisotropic CASPT2 (ATZ) potential; lower solid line: results for anisotropic "full-CI Morse potential" of Eq. (2.4) with fitted $C/D = 2.5$, see text).

(an extension to 130–3000 K is provided by $k_{rec,\infty} \approx 3.34 \times 10^{-10}$ $(T/300\ \mathrm{K})^{0.186}$ $\exp(-T/25200\ \mathrm{K})$ $\mathrm{cm^3\ molecule^{-1}\ s^{-1}}$). This result later on will be compared with experimental values obtained by extrapolation of falloff curves. A temperature independent value of $k_{rec,\infty} = 3.5 \times 10^{-10}$ $\mathrm{cm^3\ molecule^{-1}\ s^{-1}}$ over the range 300–2000 K was recommended in the evaluation of Ref. 2 (with an estimated accuracy of a factor of two). The present calculations are essentially in agreement with this recommendation.

When high pressure dissociation rate constants $k_{dis,\infty}$ are needed, the values of Eq. (3.7) have to be combined with the equilibrium constants $K_c = k_{rec}/k_{dis}$. Uncertainties in K_c, which mostly arise from differences in the used dissociation energies of CH_4, then may influence the conversion of $k_{rec,\infty}$ into $k_{dis,\infty}$ such as emphasized in Ref. 16. (Differences between the recommended rate constants from Ref. 2 at 1000–2000 K and calculated values from Ref. 6, see Fig. 8 from Ref. 6, evidently were exclusively due to differences in K_c and did not arise from different modelings of k_{rec}). For this reason, it appears advisable to specify which equilibrium constants K_c are used together with k_{rec}, or which dissociation energy $D_0{}^o$ of methane has been used in modeling k_{dis}

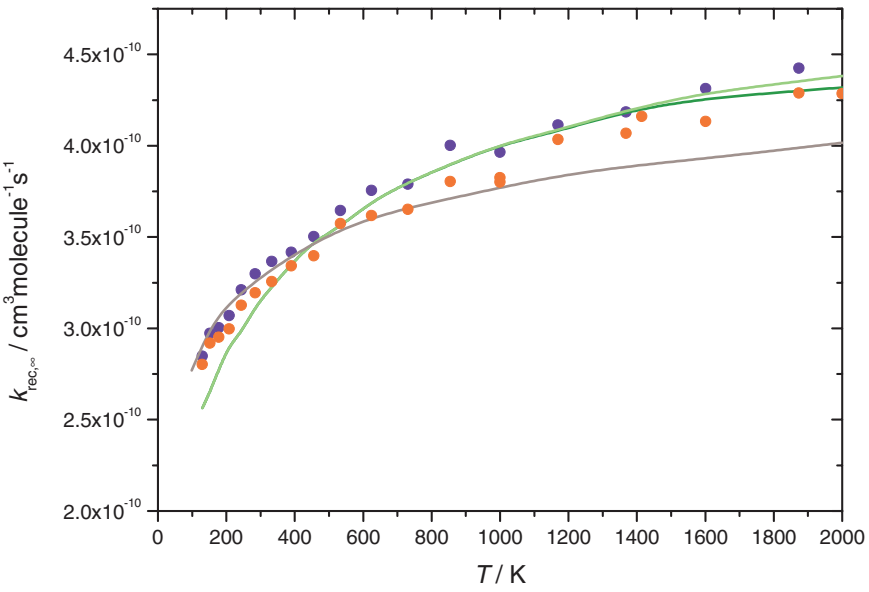

FIG. 7. Limiting high pressure recombination rate constants $k_{rec,\infty}$ (upper points: CASPT2 (ATZ) potential; lower points: CASPT2 (ADZ) potential; solid lines from top to bottom: "full-CI Morse potential" of Eq. (2.4) with $C/D = 2.5$, capture radius $r_{capt} = 2.97$ a.u.; capture radius $r_{capt} = 3.6$ a.u.; TST results with CASPT2 (ADZ) potential from Refs. 4 and 5 using a dynamical recrossing factor of 0.9, see text).

(in both cases one may prefer to split off a factor $\exp(-D_0{}^o/\mathrm{kT})$ to allow for modifications of $D_0{}^o$). At the present stage, we rely on $D_0{}^o(\mathrm{H–CH_3}) = 432.72$ ($\pm$0.14) kJ mol^{-1} from Ref. 28 (corresponding to $D_0{}^o/R = 52\,044$ ($\pm$17) K, or $D_0{}^o/\mathrm{hc} = 36\,173$ ($\pm$12) cm^{-1}, see the Appendix). With the molecular constants given in the Appendix, in rigid rotor/harmonic oscillator approximation, this leads to equilibrium constants

$$K_C = \exp(52044\,\mathrm{K}/T)\,[10^{-24.65}(T/300\,\mathrm{K})^{-1.76} + 10^{-26.38}(T/300\,\mathrm{K})^{0.67}]\,\mathrm{cm}^3\ \mathrm{molecule}^{-1}. \quad (3.8)$$

(In calculating K_c, anharmonicity in part is taken care of by employing experimental fundamental rather than harmonic frequencies; additional anharmonicity effects from higher order anharmonicity coefficients were found to be negligible compared to other uncertainties, see below.) The representation by Eq. (3.8) agrees with the numerical values within better than 2% over the range 300–5000 K. The agreement with the values given in Refs. 3 and 28 over the range 900–4000 K is better than 5%. The much larger uncertainty between various equilibrium constants alerted in Ref. 16 thus is reduced.

IV. SPECIFIC RATE CONSTANTS *k(E, J)* FOR $CH_4 \rightarrow H + CH_3$

The number of open channels $W(E, J)$ of Eq. (2.2), derived by the trajectory calculations of Sec. II, forms an important part of the specific rate constants $k(E, J)$ for dissociation as given by statistical unimolecular rate theory

$$k(E, J) = W(E, J)/h\rho(E, J). \quad (4.1)$$

It therefore appears appealing to extend our treatment of $W(E, J)$ towards $k(E, J)$. The calculation of the rovibrational densities of states $\rho(E, J)$ for spherical top CH_4 in rigid rotor-harmonic oscillator approximation is straightforward and can, e.g., be done with the Whitten-Rabinovitch approximation $\rho^{WR}_{vib,h}(E_{vib})$ leading to

$$\rho\,(E, J) = (2J + 1)\,\rho^{WR}_{vib,h}\,(E_{vib})\,F_{anh}\,(E, J) \quad (4.2)$$

(with $E_{vib} = E + D_0{}^o - B_eJ(J+1)$ where B_e = rotational constant of CH_4 and $D_0(J = 0)/\mathrm{hc} = 36\,173$ cm^{-1}, see the Appendix; $W(E, J)$ includes a symmetry number $\sigma = 6$ for CH_3 while $\rho^{WR}_{vib,h}(E_{vib})$ includes a symmetry number $\sigma = 12$ for CH_4).

A less well understood contribution to $\rho(E, J)$ is the anharmonicity factor $F_{anh}(E, J)$. We have employed the empirical method proposed in Ref. 30 and tested in Ref. 31. This method takes into account Morse anharmonicities in the stretching vibrations and empirical models for the coupling between deformation and stretching vibrations (we have used the optimum parameters $c = 0.5$ and $n = 0.41$ in Eq. (2.4) of Ref. 30). The resulting anharmonicity factors $F_{anh}(E_{vib})$ are shown in Fig. 8. For the dissociation energy $D_0{}^o/\mathrm{hc} = 36\,173$ cm^{-1}, we obtained $F_{anh} = 1.54$. This value is close to the values determined in Refs. 32 and 33. (In comparing the present anharmonicity factors with those from Nguyen and Barker,[32] one should notice that these authors referred their anharmonic numbers of states to calculations with harmonic frequencies.

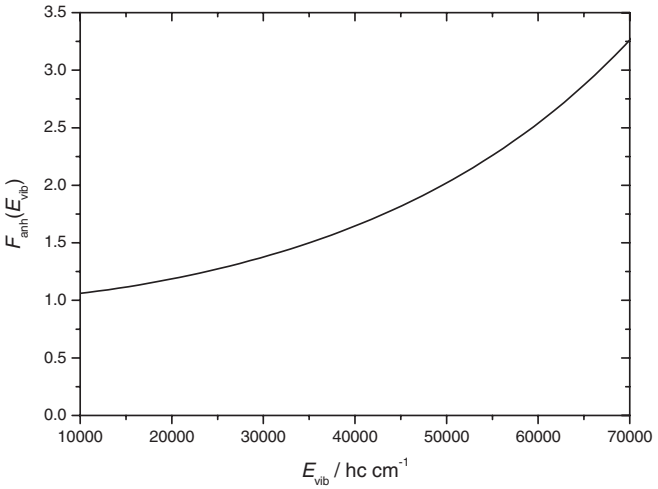

FIG. 8. Anharmonicity corrections $F_{anh}(E)$ to the vibrational density of states of CH_4 in Eq. (4.2) (for $J = 0$; empirical results as represented by Eq. (4.3); $\rho_{vib,h}$ calculated with fundamental frequencies, see text).

We prefer to refer to calculations with the experimental fundamental frequencies, see the Appendix; in this way, that part of the anharmonicity which is contained in the zero point energy is accounted for separately.) Our anharmonicity factor $F_{anh}(E, J)$ to be included in Eq. (4.1) then can be approximated by

$$F_{anh}(E_{vib}) \approx \exp[(E_{vib}/62\,800\,\mathrm{cm}^{-1}\,\mathrm{hc})^{1.544}]. \quad (4.3)$$

Combining $W(E, J)$, $\rho^{WR}_{vib,h}(E_{vib})$, and $F_{anh}(E_{vib})$ through Eq. (4.1) leads to $k(E, J)$ as illustrated in Fig. 9. One notices the usual pattern of energy and angular momentum dependences which is governed by the different contributions of the centrifugal barriers $E_0(J)$, the number of open channels $W(E,J)$, and the rovibrational densities of states.

V. BROADENING FACTORS IN FALLOFF REPRESENTATIONS

In the following, we choose the doubly reduced representation[25] of the rate constants k (for recombination or dissociation) as a function of the reduced pressure scale x

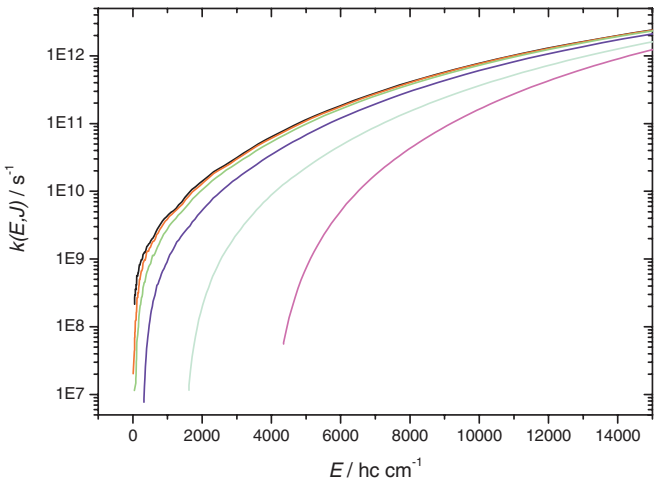

FIG. 9. Specific rate constants $k(E, J)$ for methane dissociation from Eq. (4.1) (curves from top to bottom: $J = 0$, 5, 10, 20, 40, and 60).

defined by

$$x = k_0/k_\infty \propto [\mathrm{M}] \tag{5.1}$$

(k_0 is the pressure-proportional limiting low pressure rate constant). The rate constant k then is expressed as

$$k/k_\infty = [x/(x+1)]F(x) \tag{5.2}$$

with the broadening factor $F(x)$.

We first consider strong collision broadening factors $F^{sc}(x)$. According to Refs. 12 and 13, these are related to $W(E, J)$ and $\rho(E, J)$ by

$$F^{sc}(x) = (1+x)\sum_{J=0}^{\infty}(2J+1)\int_{E_0(J)}^{\infty}[F_\rho F_W/(xF_\rho + F_W)] \times \exp(-E/kT)d(E/kT) \tag{5.3}$$

with

$$\rho(E, J)/F_\rho = \sum_{J=0}^{\infty}\int_{E_0(J)}^{\infty}(2J+1)\rho(E, J) \times \exp(-E/kT)d(E/kT) \tag{5.4}$$

and

$$W(E, J)/F_W = \sum_{J=0}^{\infty}\int_{E_0(J)}^{\infty}(2J+1)W(E, J) \times \exp(-E/kT)d(E/kT). \tag{5.5}$$

As we have $W(E, J)$ from Sec. II and $\rho(E, J)$ from Sec. IV, $F^{sc}(x)$ can be determined. The results are shown in Fig. 10. There is only little temperature dependence of the strong collision broadening factors $F^{sc}(x)$. One also notices a considerable amount of asymmetry relative to the "center of the falloff curve" at $x = 1$ (denoted by the subscript c).

There are various ways to represent $F^{sc}(x)$ in analytical form. We have compared these representations in Ref. 14. There is first the conventional "symmetric broadening factor" (i.e., $F^{sc}(x) = F^{sc}(-x)$) from Ref. 25,

$$F^{sc}(x) \approx F_c^{1/[1+(\log x/N^{sc})]^2} \tag{5.6}$$

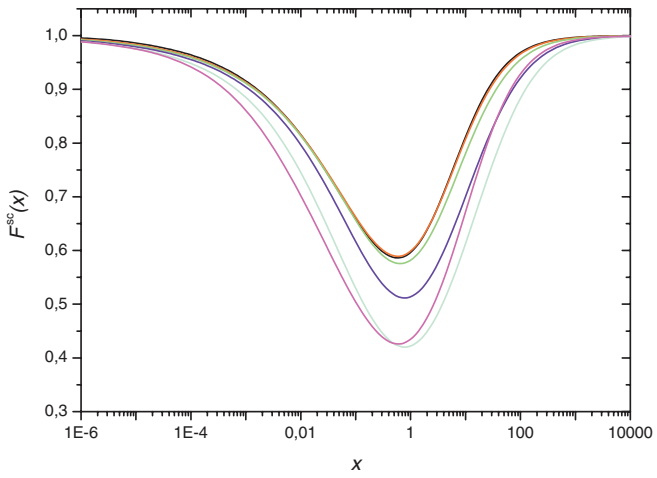

FIG. 10. Strong collision broadening factors $F^{sc}(x)$ with $x = k_0/k_\infty$ from Eqs. (5.3)–(5.5) (curves with minima from bottom to top for $T = 2000$, 4000, 1000, 500, 150, and 300 K).

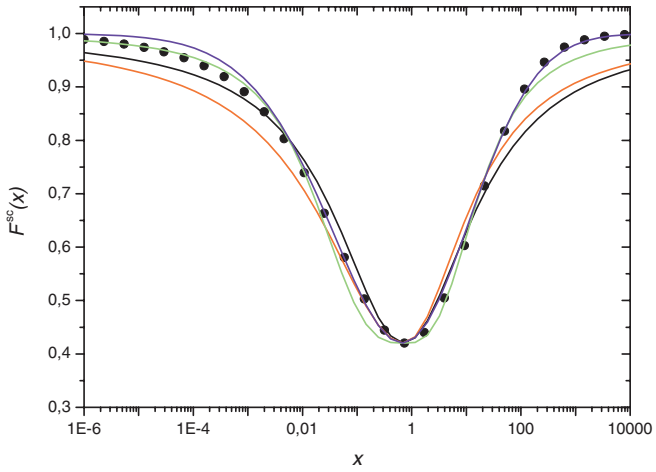

FIG. 11. Representation of strong collision broadening factors $F^{sc}(x)$ from Fig. 10 by approximate expressions ($T = 2000$ K; points: results for the CASPT2 potential; full lines from bottom to top at the right side: Eq. (5.6), Eq. (6.1) from Ref. 14, Eqs. (5.8) and (5.9); at the left side: Eq. (6.1) from Ref. 14, Eqs. (5.6), (5.8) and (5.9)).

with the width

$$N^{SC} \approx 0.75 - 1.27 \log F_C^{SC}. \tag{5.7}$$

For the example of $T = 2000$ K, where $F_c{}^{sc}$ is calculated as 0.42, Fig. 11 compares the calculations from the present work (for the CASPT2(ATZ) potential) with the representation by Eq. (5.6). There is fairly good agreement at the low pressure side $x < 1$, but Eq. (5.6) gives too broad falloff curves at the high pressure side $x > 1$. Figure 11 also includes representations with asymmetric broadening factors (i.e., $F^{sc}(x) \neq F^{sc}(-x)$) as proposed in Ref. 14 using Eqs. (6.1)–(6.3) from that reference. The minimum of $F^{sc}(x)$ now is shifted from $x = 1$ to about $x \approx 0.7$. At the low pressure side apparently Eq. (6.2) from Ref. 14 gives the best agreement with the calculated points. This representation is given by

$$F^{sc}(x) \approx F_c^{1/\{1+[|\log(1.4x)|/(N+\Delta N)]^2\}} \tag{5.8}$$

with N from Eq. (5.7) and $\Delta N = -0.65 \log F_c$ for $\log(1.4x) < 0$). On the other hand, Eq. (6.3) from Ref. 14 accounts slightly better for the narrowing of the falloff curve at the high pressure side, see Fig. 11. This representation is given by

$$F^{sc}(x) \approx 1 - (1 - F_c)\exp\{-[\log(1.5x)/N]^2/N^*\} \tag{5.9}$$

with N from Eq. (5.7), $N^* = 2$ for $\log(1.5x) > 0$, and $N^* = 2[1-0.15 \log(1.5x)]$ for $\log(1.5x) < 0$. Comparing the various representations, one may decide on practical grounds which representation should be preferred. However, Eq. (5.9) apparently provides the best representation over the full falloff curve.

Besides strong collision broadening of the falloff curves, there is additional broadening by weak collisions. We have analyzed this in detail in Ref. 14. Weak collision broadening factors $F^{wc}(x)$ have a similar form as $F^{sc}(x)$ such that we suggest to employ Eq. (5.2) with a common $F(x)$ and center broadening factors given by

$$F_c \approx F_c^{sc} F_c^{wc}. \tag{5.10}$$

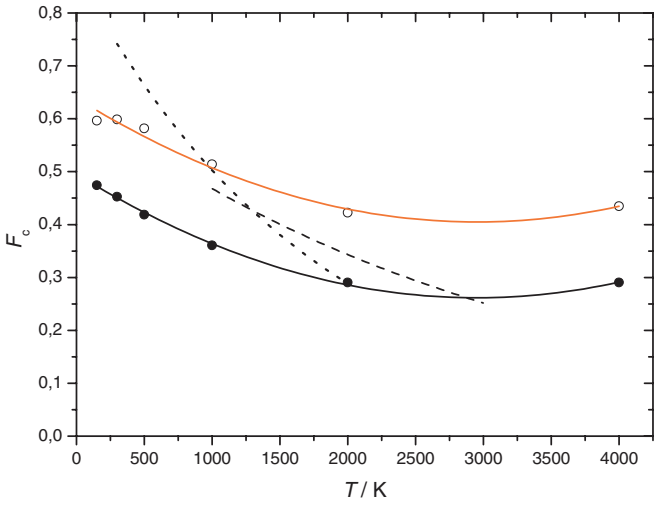

FIG. 12. Center broadening factors F_c (open circles: F_c^{sc} and red line: representation by Eq. (5.13); filled circles: $F_c = F_c^{sc}F_c^{wc}$ for M = Ar and black line: representation by Eq. (5.14); dashed line: simplified SACM model from Ref. 15; dotted line: RRKM/master equation model from Ref. 16).

F_c^{wc} depends on the efficiency of collisional energy transfer, i.e., on the "weakness of the collisions" as expressed by $\langle\Delta E\rangle$ or the related low pressure collision efficiency β_c (see Sec. VI), connected to $\langle\Delta E\rangle$ through[18]

$$\frac{\beta_c}{1-\sqrt{\beta_c}} \approx \frac{-\langle\Delta E\rangle}{F_E kT}. \tag{5.11}$$

We found that F_c^{wc} decreases with decreasing β_c according to[14,25]

$$F_c^{wc} \approx \max\left\{\beta_c^{0.14}, 0.64\,(\pm 0.03)\right\} \tag{5.12}$$

until it levels off at a limiting value near 0.64 (Figs. 12 and 13 of Ref. 14 more precisely describe the transition between $\beta_c^{0.14}$ and 0.64). The broadening factors besides the strong collision broadening thus also depend on the collision efficiency β_c of the bath gas.

We conclude this section by inspecting the temperature dependence of the center broadening factors F_c from Eq. (5.10). We first consider the bath gas-independent strong collision broadening factor F_c^{sc}. The results in Fig. 12 show only a weak temperature dependence, with F_c varying between 0.61 at 150 K and 0.43 at 4000 K. We mention that the results within about 10% do not change when anharmonic densities of states are replaced by harmonic values, r_e and β in Eq. (2.4) are changed by a factor of 2, or Eq. (2.4) is exchanged by the CASPT2 potential. F_c^{sc} thus is very insensitive to most details of the dynamics. An analytical approximation to F_c^{sc} in the form

$$F_c^{sc} \approx 0.405 + [(T - 2950\,\mathrm{K})/6100\,\mathrm{K}]^2 \tag{5.13}$$

is included in the figure. On the other hand, the additional weak collision factors F_c^{wc} from Eq. (5.12) (or the graphical representation of Figs. 12 and 13 in Ref. 14) are bath gas-dependent. In order to estimate these, one needs to know $\langle\Delta E\rangle$ for energy transfer and F_E in Eq. (5.11), see Sec. VI. For demonstration, we use the value of $-\langle\Delta E\rangle/\mathrm{hc} \approx 50\ \mathrm{cm}^{-1}$ such as obtained, for M = Ar, in Ref. 17. This leads to $F_c^{wc} \approx 0.76$, 0.70, and 0.67, for $T = 300$, 1000, and 2000 K, respectively, such that $F_c = F_c^{sc}F_c^{wc} \approx 0.45$, 0.36, and 0.29. Recommendations of F_c for M = Ar from simpler treatments are included in Fig. 12. The simplified SACM approach (including weak collision effects) of Ref. 15 led to $F_c \approx \exp(-0.45 - T/3230\ \mathrm{K})$ between 1000 and 3000 K, i.e., $F_c = 0.47$ and 0.34 at 1000 and 2000 K, while the RRKM/master equation approach of Ref. 16 gave $F_c \approx 0.876\exp(-T/1801\ \mathrm{K}) + 0.124\exp(-T/33.1\ \mathrm{K})$ between 300 and 2000 K, i.e., $F_c = 0.74$, 0.50, and 0.29 for $T/\mathrm{K} = 300$, 1000, and 2000 K, respectively. Up to about 2000 K, the present values of F_c thus are smaller than the recommendations of Refs. 2, 15, and 16 and have a weaker temperature dependence. The results for M = Ar (with $-\langle\Delta E\rangle/\mathrm{hc} \approx 50\ \mathrm{cm}^{-1}$) in Fig. 12 are well represented by

$$F_c \approx 0.262 + [(T - 2950\,\mathrm{K})/6100\,\mathrm{K}]^2. \tag{5.14}$$

Further elaboration of F_c^{wc}, and hence the total F_c, requires the detailed analysis of experimental limiting low pressure rate constants $k_{rec,0}$ or $k_{dis,0}$ with respect to the values of $\langle\Delta E\rangle$ such as given in Sec. VI, or reference to the theoretical determinations of $\langle\Delta E\rangle$ from Ref. 7.

VI. LOW PRESSURE DISSOCIATION RATE CONSTANTS $k_{dis,0}$

According to unimolecular rate theory, the limiting low pressure rate constant for dissociation $k_{dis,0}$ can be split into two parts,

$$k_{dis,0} = [\mathrm{M}]Z\beta_c f^* \tag{6.1}$$

with a statistical factor f^* given by the equilibrium population of dissociative states. In detail, f^* writes

$$f^* = \sum_{J=0}^{\infty}(2J+1)\int_{E_0(J)}^{\infty} dE f(E,J). \tag{6.2}$$

The collision energy transfer part [M] $Z\,\beta_c$, with a collision frequency Z and a collision efficiency β_c, has to be determined by master equation solution,[18] see below.

The statistical factor can approximately be further factorized in the form

$$f^* \approx \rho_{vib,h}(E_0)kT\,F_E F_{anh} F_{rot}\exp(-E_0/kT)/Q_{vib} \tag{6.3}$$

(for the meaning of the factors, see Refs. 21 and 25). After the present determination of the centrifugal barriers $E_0(J)$ for the relevant potential energy surface, see Eq. (2.5), the rotational factor F_{rot} can be determined following Eqs. (14)–(19) of Ref. 25. In addition, our treatment of the anharmonicity factor $F_{anh}(E_{vib})$ from Eq. (4.3) allows us to specify $F_{anh} \approx F_{anh}(E_0)$ (the energy dependence of the effective F_{anh} can be included in the factor $F_{E,}$, see below). With these refinements in the calculation of the statistical factor, an improved analysis (compared to Refs. 15 and 17) of experimental $k_{dis,0}$ with respect to the product [M]$Z\ \beta_c$ in Eq. (6.1) can be made. We, therefore, have reevaluated f^* which leads to the

TABLE I. Falloff corrections and energy transfer parameters from low pressure dissociation experiments in M = Ar ($\langle\Delta E\rangle$ and α: experimental values from analysis of experimental $k_{dis,0}$; α_{th} : theoretical value from Ref. 7, see text).

References	T (K)	[Ar] (10^{18} molecule cm^{-3})	$k_{dis}/k_{dis,0}$	F_E	$-\langle\Delta E\rangle$ (hc cm^{-1})	α (cm^{-1})	α_{th} (cm^{-1})
This work	2200	2–800	0.8–0.2	1.41	59	388	512
Reference 45	2200	~2	~0.8	1.41	~60	~390	512
Reference 46	3000	2	0.9	1.63	74	540	647
Reference 46	4000	1	0.97	2.00	82	719	802

following result:

$$f^* \exp(-E_0/kT) = F(T), \tag{6.4}$$

where $\log[F/T)/F(300\ \mathrm{K})] \approx -a[\log(T/300\ \mathrm{K})]^n$ with $F(300\ \mathrm{K}) = 2.245 \times 10^7$, $a = 2.105$, and $n = 2.62$ for $T = 300$–3000 K ($n = 2.35$ applies for $T = 300$–5000 K). (More accurate numbers of f^* than fitted by Eq. (6.4) are given in the Appendix.) As f^* most sensitively depends on the bond energy E_0, the equilibrium constant K_c from Eq. (3.8) has to be determined with the same E_0 to avoid internal inconsistencies. It appears, therefore, useful like in Eq. (3.8) to split off the factor $\exp(-E_0/kT)$ in Eq. (6.4).

Having specified f^* and identifying Z with the Lennard-Jones collision frequency Z_{LJ}, the relation between the collision efficiency β_c and $k_{dis,0}$ can be analyzed. Through Eq. (5.12), this leads to the average total energy transferred per collision $\langle\Delta E\rangle$. For an exponential collision model, $\langle\Delta E\rangle$ is approximately related to $\langle\Delta E_d\rangle$, the average energy transferred in down collisions, through[18]

$$\langle\Delta E\rangle \approx -\left\langle\Delta E_d^2\right\rangle/(\langle\Delta E_d\rangle + F_E kT) \tag{6.5}$$

such that

$$\beta_c \approx [\langle\Delta E_d\rangle/(\langle\Delta E_d\rangle + F_E kT)]^2. \tag{6.6}$$

The factor F_E, forcing up- and down-transitions near E_0 into detailed balance, is approximately given by

$$F_E \approx \sum_{i=0}^{s-1} \frac{(s-1)!}{(s-1-i)!}\left[\frac{kT}{E_0 + a(E_0)E_z}\right]^i \tag{6.7}$$

with the Whitten-Rabinovitch correction factor $a(E_0)$ and the vibrational zero point energy E_z of CH_4, see Ref. 25. Implementing the energy dependence of the anharmonicity factor $F_{anh}(E)$ from Eq. (4.3) into the derivation of F_E, accidentally, in this case can be accounted for by increasing s in Eq. (6.7) by unity. F_E then has the values 1.04, 1.16, 1.36, 1.63, 1.99, and 2.49, for T/K = 300, 1000, 2000, 3000, 4000, and 5000, respectively. For fundamental reasons, it is preferable to work with $\langle\Delta E\rangle$ and not with $\langle\Delta E_d\rangle$, because the solution of the present type of master equations only depends[18,34,35] on the first and second moments of energy transfer, $\langle\Delta E\rangle$ and $\langle\Delta E^2\rangle$, respectively. For numerical reasons, one may prefer $\langle\Delta E_d\rangle$ and link the results through Eqs. (6.5) and (6.6). These relationships will be used in the following if either β_c is predicted on the basis of theoretical values for $\langle\Delta E_d\rangle$ from Refs. 6 and 7 or experimental values for β_c are further analyzed with respect to $\langle\Delta E\rangle$ and $\langle\Delta E_d\rangle$.

Before we analyze experimental $k_{dis,0}$, we take advantage of the detailed calculations of $\langle\Delta E_d\rangle$ from Ref. 7 for M = He, Ne, Ar, Kr, H_2, N_2, CO, and CH_4. Here, down-step sizes were expressed in the form

$$\alpha(T) = \alpha_{300}(T/300\ \mathrm{K})^n. \tag{6.8}$$

It should be emphasized that $\langle\Delta E_d\rangle$ and α are not identical for a number of reasons (energy and rotational dependences, truncation of the energy scale at the vibrational ground state of CH_4, average account for detailed balancing near E_0, see Ref. 36). However, the differences are probably not larger than the calculational or experimental uncertainties. Identifying $\alpha(T)$ with $\langle\Delta E_d\rangle$ and using Eqs. (6.5)–(6.8), therefore, we obtain theoretical values of $\langle\Delta E\rangle$ summarized in Table I. At the same time, with f^* from Eq. (6.4), we obtain fully theoretical values of $k_{dis,0}$. The combination with Eq. (3.8) gives the corresponding $k_{rec,0}$.

The values of $k_{dis,0}$ and $k_{rec,0}$ cannot immediately be compared with experimental values. The analysis of experimental data shows that none of the experiments were conducted close enough to the low pressure limit that substantial falloff corrections were not required. Therefore, a careful analysis of the full falloff curves for all experimental studies has to be done. This is the issue of Sec. VII where we compare fully theoretical values of $k_{dis,0}$ and $k_{rec,0}$ with experimental falloff-corrected values. Agreement finally is achieved when α_{300} or $\langle\Delta E_d\rangle$ are slightly modified which results in "experimental values" of these quantities.

VII. COMPARISON OF EXPERIMENTAL AND THEORETICAL LOW PRESSURE RATE CONSTANTS

The results of the theoretical work summarized in Secs. II–VI, which was nearly completely based on *ab initio* potentials and the intra- and intermolecular dynamics on such potentials, may serve for a complete theoretical modeling of the rate constants as function of temperature, pressure, and nature of the bath gas. The comparison with experimental results then becomes interesting in many ways. On the one hand, the extent of falloff corrections of the measured rate constants can be specified much better than by extrapolation of experimental data. On the other hand, the least certain theoretical details can be identified and a fine-tuning of the theoretical results can be made. This in turn leads to refinements of previously recommended rate constants such as those given in Ref. 2.

Previous evaluations of experimental results for k_{dis} and k_{rec} (see Refs. 2, 6, 7, 15, and 16) all demonstrated more or less good agreement between measured and modeled rate constants. However, most of the representations left

something to desire. Sometimes the results were only shown in graphical form without giving details about the limiting rate constants or the underlying equilibrium constants, such that extrapolations to general conditions were difficult to do. Sometimes simplified falloff treatments were employed such that considerable differences of the falloff parameters were obtained, see Fig. 12; the effects of these simplifications then were compensated by choosing different energy transfer parameters. Also, the sensitivity of the modeling with respect to the different input parameters and their uncertainties was not analyzed in particular. Nevertheless, the previously recommended rate constants were of considerable practical value, allowing for inter- and extrapolations of measured results to conditions not studied before. With the results of the present work one can arrive at refinements both on the theoretical and on the experimental side of the analysis of the reaction.

By comparing experimental and theoretical falloff curves, we first realize that all experiments needed falloff extrapolations to the limiting rate constants, most of the falloff corrections being more substantial then assumed. For instance, it will be shown in the following that all of the available high temperature dissociation experiments, which were considered as limiting low pressure studies, require non-negligible falloff corrections. Analyzing experimental results, we further have to identify the least certain modeling parameters. Although this involves some guesswork, one may be relatively certain for most of the parameters. For example, we think that the equilibrium constants K_c from Eq. (3.8) over the range 300–5000 K are accurate to within better than 5%. High pressure recombination rate constants $k_{rec,\infty}$ from Eq. (3.7) over the range 130–3000 K are believed to be accurate within about 10%. Considering the individual uncertainties of the factors contributing to $f^* \exp(E_0/kT)$ from Eq. (6.4), we estimate an accuracy of this quantity of better than 5%. Figures 10 and 11 demonstrate variations of the strong collision falloff broadening factors $F^{sc}(x)$ and possible uncertainties of the chosen falloff representations which also are in the percent range. Weak collision broadening effects have similar uncertainties. By combining these effects, cumulated uncertainties for $F(x)$ of the order of 10% appear probable. Tentatively at this stage, we attribute the remaining differences between experimental and theoretical rate constants to uncertainties in the theoretical energy transfer parameters which are believed to be of the order of 10%–20%. The agreement within about 10%–30% between calculated average energies transferred per collision from Ref. 7 and values obtained by our analysis of experimental data, see below, then appears most encouraging.

In comparing experiments and theory, we first demonstrate the non-uniqueness of the modeling of falloff curves. We have chosen dissociation experiments near 2200 K in the bath gas Ar, see Fig. 13. There is one group of experiments at lower pressures ([Ar] in the range 2×10^{18}–2×10^{19} molecule cm^{-3}) from Refs. 37–43 which often were assumed to correspond to the low pressure limit of the reaction. Only few experiments reached further up towards the high pressure range ([Ar] up to 10^{21} molecule cm^{-3}, data from Ref. 15 reevaluating experiments from Ref. 44). Figure 13 compares two possibilities to fit the experimental data to a falloff curve

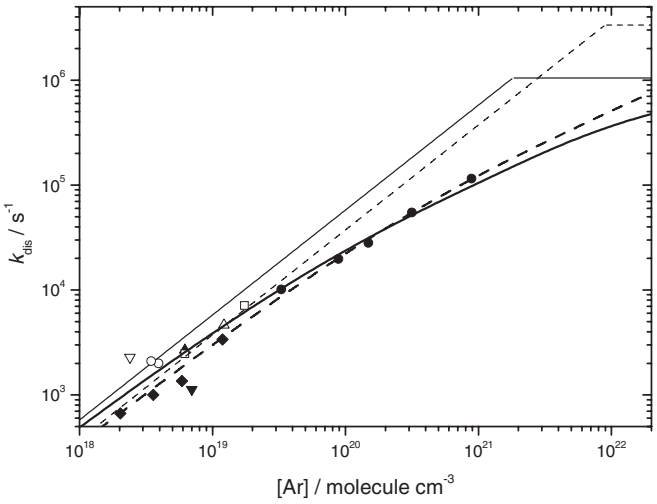

FIG. 13. Falloff curves for CH_4 (+ Ar) → CH_3 + H (+ Ar) at $T = 2200$ K (experimental points: full circles from Ref. 15 reevaluating Ref. 44, open squares: Ref. 37, open triangle: Ref. 38, diamonds: Ref. 43, filled triangle: Ref. 39, filled inverted triangle: Ref. 40, open circles: Ref. 40, open inverted triangle: Ref. 41, solid lines: fitted falloff curve with limiting rate constants for fixed $k_{dis,\infty} = 1.05 \times 10^6$ s^{-1}, and dashed lines: fitted falloff curve for freely varied $k_{dis,\infty} = 3.3 \times 10^6$ s^{-1}, see text).

where the center broadening factor F_c was fixed to the theoretical value of $F_c = 0.28$ from Eq. (5.14). By fixing $k_{dis,\infty}$ to 1.05×10^6 s^{-1} (as obtained from $k_{rec,\infty}$ from Eq. (3.7) and K_c from Eq. (3.8)), $k_{dis,0} \approx$ [Ar] 5.8×10^{-16} cm^3 molecule^{-1} s^{-1} is fitted by least mean-squares fit to all experimental points shown in Fig. 13, see solid lines in Fig. 13. Leaving $k_{rec,\infty}$ as a second fit parameter, would have given $k_{dis,\infty} = 3.3 \times 10^6$ s^{-1} and $k_{dis,0} =$ [Ar] 3.7×10^{-16} cm^3 molecule^{-1} s^{-1}, see dashed lines in Fig. 13. As the former fit leads to energy transfer parameters in much closer agreement with theory, see below, and consistency with the high pressure recombination rate constants has been forced, clearly the former fit is preferable and the non-uniqueness is removed.

Except for Fig. 13, we renounce on further comparisons of measured and modeled falloff curves. Instead, in Table I we analyze representative experimental data for M = Ar with respect to falloff corrections to low pressure rate constants and the derived energy transfer parameters in comparison to the theoretical values from Ref. 7. A number of observations are made: (i) Falloff corrections are needed everywhere, even at the highest temperatures where the experiments are closest to the low pressure limit. (ii) The derived total energies $\langle \Delta E \rangle$ transferred per collision are only weakly dependent on the temperature (at least for M = Ar where a sufficiently broad temperature range has been studied). This conclusion confirms the results from Ref. 17 where a similar value of $\langle \Delta E \rangle$ was derived. The only weak T-dependence of $\langle \Delta E \rangle$ is consistent with the magnitude of the T-dependence of $\alpha(T)$ from the theoretical work of Ref. 7, see Eq. (6.8). (iii) The values of $\alpha(T)$ from the theoretical work are about 20(±10)% larger than the values deduced in the present work from the analysis of the experimental low pressure rate constants. This is certainly within the uncertainty of either approach and should be considered as very good agreement. (iv) Relying on the temperature dependence of the theoretical α, but reducing

TABLE II. Recommended rate parameters for falloff curves of CH_4 (+Ar) ⇔ CH_3 + H (+Ar) (ranges 130–3000 K for $k_{rec,\infty}$, 100–5000 for $k_{rec,0}$, 100–4000 K for F_c, 300–5000 K for K_c, see text).

$k_{rec,\infty} = 3.34 \times 10^{-10}\ (T/300\ \mathrm{K})^{0.186}\ \exp(-T/25\ 200\ \mathrm{K})\ \mathrm{cm^3\ molecule^{-1}\ s^{-1}}$.
$k_{rec,0} = [\mathrm{Ar}]\ 10^{-26.19}\ \exp[-(T/21.22\ \mathrm{K})^{0.5}]\ \mathrm{cm^6\ molecule^{-2}\ s^{-1}}$.
$F_c = 0.262 + [(T-2950\ \mathrm{K})/6100\ \mathrm{K}]^2$.
$K_c = \exp(52\ 044\ \mathrm{K}/T)\ [10^{-24.65}\ (T/300\ \mathrm{K})^{-1.76} + 10^{-26.38}\ (T/300\ \mathrm{K})^{0.67}]\ \mathrm{cm^3\ molecule^1\ s^{-1}}$.
$k/k_\infty = xF(x)/(1+x)$ with $x = k_0/k_\infty$.
$F(x) \approx 1-(1-F_c)\ \exp\{-[\log(1.5x)/N]^2/N^*\}$ with $N = 0.75–1.27\ \log F_c$, $N^* = 2$ for $\log(1.5x) > 0$, and $N^* = 2[1-0.15\ \log(1.5\ x)]$ for $\log(1.5\ x) < 0$.

the absolute value of α_{300} in Eq. (6.8) by a factor of 1.2 to 96 $\mathrm{cm^{-1}}$ (a compromise between the present analysis of Fig. 13 and the high temperature data from Ref. 46), one obtains modeled low pressure recombination rate constants $k_{rec,0}$ in M = Ar which between 100 and 5000 K can be represented by

$$k_{rec,0} = [\mathrm{Ar}]10^{-26.14} \times \exp[-(T/21.38\ \mathrm{K})^{0.5}]\ \mathrm{cm^6 molecule^{-2}\ s^{-1}}. \quad (7.1)$$

Reducing α_{300} to 87 $\mathrm{cm^{-1}}$, which corresponds to the low pressure limit of Fig. 13, would lead to the alternative

$$k_{rec,0} = [\mathrm{Ar}]10^{-26.19} \times \exp[-(T/21.22\mathrm{K})^{0.5}]\ \mathrm{cm^6 molecule^{-2}\ s^{-1}}. \quad (7.2)$$

VIII. CONCLUSIONS AND RECOMMENDED RATE CONSTANTS

The present SACM/CT modeling of the limiting high pressure recombination rate constants $k_{rec,\infty}$ led to values represented by Eq. (3.7) and Fig. 7. The values obtained are consistent with the falloff extrapolation of Fig. 13 and similar extrapolations of data from Refs. 47 and 48, such as documented in Refs. 6, 7, 15, and 16, although the databases were more limited. Only the low temperature recombination experiment at 300 K from Ref. 49, being conducted in M = CH_4 far up into the high pressure range, could be safely extrapolated to $k_{rec,\infty}$ and led to a value very close to our calculated result. Measurements from Ref. 50 over the range 300–600 K showed a number of inconsistencies such that falloff extrapolations towards $k_{rec,\infty}$ were difficult to do. As our calculated values are also perfectly consistent with isotope exchange data in the CH_xD_{4-x}-system, see Refs. 51 and 52, Eq. (3.7) is recommended for practical applications. Together with the equilibrium constant K_c from Eq. (3.8), $k_{rec,\infty}$ can also safely be converted to $k_{dis,\infty}$.

Low pressure rate constants $k_{rec,0}$ and $k_{dis,0}$ are slightly less well characterized, because theoretical modeling of energy transfer parameters as well as their extraction from extrapolated experimental falloff curves leads to some differences, e.g., a factor of 1.6 in $k_{dis,0}$ at 2200 K. Relying on the extrapolated low pressure value from Fig. 13 and the temperature dependence of the energy transfer parameters from the calculations of Ref. 7, leads to $k_{rec,0}$ as given in Eq. (7.2) for the bath gas Ar.

The present work provided falloff center broadening factors F_c such as given for M = Ar by Eq. (5.14), see Fig. 12. This expression is also recommended for other bath gases as long as their energy transfer parameters are not known well enough to deserve a treatment combining Eqs. (5.12) and (5.13). Figure 11 compares symmetric broadening factors $F^{sc}(x)$ in the "standard form" of Eq. (5.6) with asymmetric broadening factors like Eqs. (5.8) and (5.9) from Ref. 14. Equation (5.9) is recommended because it provides the best approach of either the low and the high pressure limits. Table II summarizes the recommended rate constants for M = Ar.

The present combination of experimental and theoretical results concludes a long history of studies which all contained fitted parameters, mostly for energy transfer.[15–17,21,44,55,56] With the work of Ref. 7 this gap in a fully theoretical analysis is closed and the methane system has reached maturity.

One finally may ask for low pressure rate constants in other bath gases than M = Ar. The experimental database at this stage is very limited, because, except for Ar and Kr, falloff curves were not extended down to sufficiently low pressures to allow for reliable falloff extrapolations on the basis of the broadening factors from the present calculations. We, therefore, have tentatively used the calculated energy transfer parameters from Ref. 7, reducing the given α_{300} for all bath gases by a factor of 1.2 such as discussed for M = Ar. This leads to values of $k_{rec,0}$ for M = N_2 and CH_4 such as represented by

$$k_{rec,0} = [\mathrm{N_2}]10^{-26.04} \times \exp[-(T/21.91\mathrm{K})^{0.5}]\ \mathrm{cm^6 molecule^{-2}\ s^{-1}}, \quad (8.1)$$

$$k_{rec,0} = [\mathrm{CH_4}]10^{-25.44} \times \exp[-(T/21.71\ \mathrm{K})^{0.5}]\ \mathrm{cm^6\ molecule^{-2}\ s^{-1}}. \quad (8.2)$$

No such information is available for M = O_2 and H_2O such that only guesses can be made at this stage. We recommend to use Eq. (8.1) also for M = O_2. On the other hand, M = H_2O is much closer to a strong collider. By analogy to our work on H + O_2 (+ H_2O) → HO_2 (+H_2O), we have modeled $k_{rec,0}$ with a Lennard-Jones collision frequency and a collision efficiency corresponding to $-\langle\Delta E\rangle/hc \approx 300\ \mathrm{cm^{-1}}$ (independent of T, corresponding to $\alpha_{300} \approx 420\ \mathrm{cm^{-1}}$ and $n \approx 0.45$) in Eq. (6.8) which leads to

$$k_{rec,0} = [\mathrm{H_2O}]10^{-25.31} \times \exp[-(T/19.52\ \mathrm{K})^{0.5}]\ \mathrm{cm^6\ molecule^{-2}\ s^{-1}}. \quad (8.3)$$

The use of the Lennard-Jones collision frequency here does not give much different results from using a collision frequency given by a dipole-quadrupole capture rate constant.[55,56] The chosen value for $\langle \Delta E \rangle$ is that found for $H + O_2$ ($+H_2O$). Clearly, more experimental and theoretical work on this aspect of the reaction is needed.

ACKNOWLEDGMENTS

We very much thank L. D. Harding for providing us details of the CASPT2 potentials, which were used in part of our work.

APPENDIX: MOLECULAR PARAMETERS

CH_4: ν_i/hc cm^{-1} = 2916.5, 1534.0 (2), 3018.7 (3), 1306 (3); $A = B = C = 5.269$ cm^{-1}, $\sigma = 12$; taken from Ref. 29.

CH_3: ν_i/hc cm^{-1} = 3004.42, 606.453, 3160.821 (2), 1396 (2); $A = B = 9.578$ cm^{-1}, $C = 4.742$ cm^{-1}, $\sigma = 6$; taken from Ref. 28.

$CH_4 \rightarrow H+CH_3$: $D_0{}^o = 432.72$ ($\pm$0.14) kJ mol^{-1} from Ref. 28, corresponding to $D_0{}^o/R = 52\,044$ ($\pm$17) K; $D_0{}^o$/hc = 36 173 ($\pm$12) cm^{-1}, ρ_{vib} $(E_0) = 1.050 \times 10^3/cm^{-1}$.

Equilibrium population of excited states from Eq. (6.4): $F(T) = f^*$ $\exp(E_0/kT)$ = (1.849, 2.178, 2.245, 2.029, 1.584, 0.9349, 0.3316, 0.1163, 0.04348, 0.01765, 0.003698, and 0.001018) $\times 10^7$ for T = 100, 200, 300, 500, 700, 1000, 1500, 2000, 2500, 3000, 4000, and 5000 K, respectively.

Lennard-Jones parameters: σ/nm = 0.3746, 0.3330, 0.3681, and 0.2641; ε/k K = 141.4, 136.5, 97.68, and 809.1; for M = CH_4, Ar, N_2, and H_2O, respectively, from Ref. 7 (for M = H_2O as used in Ref. 22).

[1] W. G. Mallard, F. Westley, J. T. Herron, R. F. Hampson, and O. H. Frizell, NIST Chemical Kinetics Database, Standard Reference Database 17, Version 7.0. Data Version 2012.02, US Department of Commerce, NIST, Gaithersburg, MD.
[2] D. L. Baulch, C. T. Bowman, C. J. Cobos, R. A. Cox, T. Just, J. A. Kerr, M. J. Pilling, D. Stocker, J. Troe, W. Tsang, R. W. Walker, and J. Warnatz, J. Phys. Chem. Ref. Data **34**, 757 (2005).
[3] J. W. Sutherland, M.-C. Su, and J. V. Michael, Int. J. Chem. Kinet. **33**, 669 (2001).
[4] S. J. Klippenstein, Y. Georgievskii, and L. B. Harding, Proc. Combust. Inst. **29**, 1229 (2002).
[5] L. B. Harding, S. J. Klippenstein, and A. W. Jasper, Phys. Chem. Chem. Phys. **9**, 4055 (2007).
[6] A. W. Jasper and J. A. Miller, J. Phys. Chem. A **113**, 5612 (2009).
[7] A. W. Jasper and J. A. Miller, J. Phys. Chem. A **115**, 6438 (2011).
[8] A. I. Maergoiz, E. E. Nikitin, J. Troe, and V. G. Ushakov, J. Chem. Phys. **108**, 5265 (1998).
[9] L. B. Harding, A. I. Maergoiz, J. Troe, and V. G. Ushakov, J. Chem. Phys. **113**, 11019 (2000).
[10] A. I. Maergoiz, E. E. Nikitin, J. Troe, and V. G. Ushakov, J. Chem. Phys. **117**, 4201 (2002).
[11] J. Troe and V. G. Ushakov, Phys. Chem. Chem. Phys. **10**, 3915 (2008).
[12] J. Troe and V. G. Ushakov, Faraday Discuss. **119**, 145 (2001).
[13] J. Troe, Int. J. Chem. Kinet. **33**, 878 (2001).
[14] J. Troe and V. G. Ushakov, J. Chem. Phys. **135**, 054304 (2011).
[15] C. J. Cobos and J. Troe, Z. Phys. Chem., Neue Folge **167**, 129 (1990).
[16] D. M. Golden, Int. J. Chem. Kinet. **40**, 310 (2008).
[17] C. J. Cobos and J. Troe, Z. Phys. Chem. **176**, 161 (1992).
[18] J. Troe, J. Chem. Phys. **66**, 4745 (1977).
[19] W. L. Hase and X. Hu, J. Phys. Chem. **92**, 4040 (1988).
[20] J. A. Miller, S. J. Klippenstein, and C. Raffy, J. Phys. Chem. A **106**, 4904 (2002).
[21] J. Troe, J. Chem. Phys. **66**, 4758 (1977).
[22] R. X. Fernandes, K. Luther, J. Troe, and V. G. Ushakov, Phys. Chem. Chem. Phys. **10**, 4313 (2008).
[23] L. B. Harding, private communication (2012).
[24] A. Dutta and C. D. Sherrill, J. Chem. Phys. **118**, 1610 (2003).
[25] J. Troe, J. Phys. Chem. **83**, 114 (1979).
[26] W. Stevens, B. Sztáray, N. Shuman, T. Baer, and J. Troe, J. Phys. Chem. A **113**, 573 (2009).
[27] J. Troe, Z. Phys. Chem. **223**, 347 (2009).
[28] B. Ruscic, J. E. Boggs, A. Burcat, A. G. Császár, J. Demaison, R. Janoschek, J. M. L. Martin, M. L. Morton, J. J. Rossi, J. F. Stanton, P. G. Szalay, P. R. Westmoreland, F. Zabel, and T. Bérces, J. Phys. Chem. Ref. Data **34**, 573 (2005).
[29] *NIST-JANAF Thermochemical Tables*, 4th ed., Journal of Physical Chemistry Reference Data, Monograph No. 9, edited by M. W. Chase (American Institute of Physics, Woodbury, 1998).
[30] J. Troe, Chem. Phys. **190**, 381 (1995).
[31] J. Troe and V. G. Ushakov, J. Phys. Chem. A **113**, 3940 (2009).
[32] T. L. Nguyen and J. R. Barker, J. Phys. Chem. A **114**, 3718 (2010).
[33] S. Schmatz, Chem. Phys. **346**, 198 (2008).
[34] N. G. van Kampen, Adv. Chem. Phys. **34**, 245 (1976).
[35] J. Troe, J. Chem. Phys. **77**, 3485 (1982).
[36] R. G. Gilbert, K. Luther, and J. Troe, Ber. Bunsen-Ges. Phys. Chem. **87**, 169 (1983).
[37] W. M. Heffington, G. E. Parks, K. G. P. Sulzmann, and S. S. Penner, Proc. Combust. Inst. **16**, 997 (1977).
[38] C. T. Bowman, Proc. Combust. Inst. **15**, 869 (1975).
[39] P. Roth and Th. Just, Ber. Bunsen-Ges. Phys. Chem. **79**, 682 (1975).
[40] W. C. Gardiner, H. Owen, T. C. Clark, J. E. Dove, S. H. Bauer, J. A. Miller, and W. J. MacLean, Proc. Combust. Inst. **15**, 857 (1975).
[41] K. Tabayashi and S. H. Bauer, Combust. Flame **34**, 63 (1978).
[42] G. A. Vompe, Zh. Fiz. Khim. **47**, 1396 (1973).
[43] D. F. Davidson, M. D. DiRosa, A. Y. Chang, R. K. Hanson, and C. T. Bowman, Proc. Combust. Inst. **24**, 589 (1992).
[44] R. Hartig, J. Troe, and H. Gg. Wagner, Proc. Combust. Inst. **13**, 147 (1971).
[45] T. Koike, M. Kudo, I. Maeda, and H. Yamada, Int. J. Chem. Kinet. **32**, 1 (2000).
[46] J. H. Kiefer and S. S. Kumaran, J. Phys. Chem. **97**, 414 (1993).
[47] C. J. Chen, M. H. Back, and R. A. Back, Can. J. Chem. **53**, 3580 (1975).
[48] R. W. Barnes, G. L. Pratt, and S. W. Wood, J. Chem. Soc., Faraday Trans. 2, **85**, 229 (1989).
[49] J. T. Cheng and C. T. Yeh, J. Phys. Chem. **81**, 1982 (1977).
[50] M. Brouard, M. T. Macpherson, and M. J. Pilling, J. Phys. Chem. **93**, 4047 (1989).
[51] P. W. Seakins, S. H. Robertson, M. J. Pilling, D. M. Wardlaw, F. L. Nesbitt, R. P. Thorn, W. A Payne, and L. J. Stief, J. Phys. Chem. A **101**, 9974 (1997).
[52] M.-C. Su and J. V. Michael, Proc. Combust. Inst. **29**, 1219 (2002).
[53] I. Boerger, H.-D. Klotz, and H.-J. Spangenberg, Z. Phys. Chem. (Leipzig) **263**, 257 (1982).
[54] A. Merkel, Ph. D. thesis at the Academy of Sciences of the GDR, Berlin (1986), see text at de.wikipedia.org/wiki/AngelaMerkel.
[55] T. Stoecklin, C. E. Dateo, and D. C. Clary, J. Chem. Soc. Faraday Trans. **87**, 1667 (1991).
[56] A. I. Maergoiz, E. E. Nikitin, J. Troe, and V. G. Ushakov, J. Chem. Phys. **105**, 6277 (1996).